Nano Research
DOI 10.1007/s12274-014-0640-7
Research Article

ISSN 1998-0124
CN 11-5974/O4

Contracted Interlayer Distance in Graphene/Sapphire Heterostructure

Shiro Entani[1] (✉), Liubov Yu. Antipina[2,3], Pavel V. Avramov[1,4], Manabu Ohtomo[1], Yoshihiro Matsumoto[1], Norie Hirao[5], Iwao Shimoyama[5], Hiroshi Naramoto[1], Yuji Baba[5], Pavel B. Sorokin[1,2,6] (✉) and Seiji Sakai[1]

[1] *Advanced Science Research Center, Japan Atomic Energy Agency, Tokai, Ibaraki 319-1195, Japan*
[2] *Technological Institute for Superhard and Novel Carbon Materials, Troitsk, Moscow 142190, Russian Federation*
[3] *Moscow Institute of Physics and Technology, Dolgoprudny, Moscow 141700, Russian Federation*
[4] *Siberian Federal University, 79 Svobodniy pr., Krasnoyarsk 660041, Russian Federation*
[5] *Quantum Beam Science Directorate, Japan Atomic Energy Agency, Tokai, Ibaraki 319-1195 Japan*
[6] *National University of Science and Technology MISiS, Moscow 119049, Russian Federation*

Received: 29 July 2014
Revised: 09 November 2014
Accepted: 13 November 2014

© Tsinghua University Press and Springer-Verlag Berlin Heidelberg 2014

KEYWORDS

graphene,
sapphire,
chemical vapor deposition,
graphene/insulator interface

ABSTRACT

Direct growth of graphene on insulators is expected to yield significant improvements in performance of graphene-based electronic and spintronic devices. In this study, we successfully reveal the atomic arrangement and electronic properties of a coherent heterostructure of single-layer graphene and α-Al_2O_3(0001). The analysis of the atomic arrangement of single-layer graphene on α-Al_2O_3(0001) revealed an apparentcontradiction. The in-plane analysis shows that single-layer graphene grows not in a single-crystalline epitaxial manner, but rather in polycrystalline form, with two strongly pronounced preferred orientations. This suggests relatively weak interfacial interactions are operative. However, we demonstrate that unusually strong physical interactions between graphene and α-Al_2O_3(0001) exist, as evidenced by the small separation between the graphene and the α-Al_2O_3(0001) surface. The interfacial interaction is shown to be dominated by the electrostatic forces involved in the graphene π-system and the unsaturated electrons of the topmost O layer of α-Al_2O_3(0001), rather than the van der Waals interactions. Such features causes graphene hole doping and enable the graphene to slide on the α-Al_2O_3(0001) surface with only a small energy barrier despite the strong interfacial interactions.

1 Introduction

Graphene has attracted considerable research attention in recent years for potential applications in nano-electronics and spintronics due to properties including quantum electronic transport, tunable band gap, and the extremely large charge carrier mobility [1–3]. A method of direct chemical vapor deposition (CVD)

Address correspondence to Shiro Entani, entani.shiro@jaea.go.jp; Pavel B. Sorokin, PBSorokin@tisnum.ru

growth of graphene on insulating substrates [4-8] is of particular importance for electronic and spintronic device applications for the following reasons. The first is to enable us to prepare large-scale graphene films across an entire substrate. This is in contrast to the conventional micromechanical exfoliation method [9], by which graphene is synthesized only in the form of small flakes. The second is to enable us to avoid the graphene transfer process, in contrast to CVD graphene grown on metal substrates. The introduction of defects, impurities, and cracks into graphene, which occurs during the transfer process, leads to significant degradation of charge and spin transport properties of devices, even though high-quality [10] and highly uniform [11] graphene can be obtained using CVD growth on metal substrates. The direct growth of graphene on insulators might solve this problem. Electronic characterization of graphene–insulator heterostructures has revealed that unintentional carrier doping can occur in graphene via the interface with the insulating substrates [12, 13]. Theoretical calculations have predicted the formation of a charge-transfer complex at the single-layer graphene (SLG)/rutile TiO_2(110) interface associated with the large difference of the work functions between graphene and titania [13]. Elucidation of the interfacial atomic structures is important for understanding the nature of the interface interactions and the resulting electronic properties, as well as for tailoring the charge transport properties.

In this study, we used normal-incidence X-ray standing wave (NIXSW) spectroscopy [14] to investigate the atomic structure of the graphene/insulator interface. This spectroscopy allows us to determine the element-specific vertical distances of the constituent atoms near the interface relative to the X-ray scattering plane in the substrate. The vertical distances are a useful criterion to evaluate of the degree of the interfacial interactions, which could provide critical information to gain insight into the structures and properties of the interface. Analysis of the contrasted standing wave (SW) profiles [15] obtained from the SLG/*c*-plane sapphire (α-Al_2O_3(0001)) substrate prepared by the direct CVD growth, shows the remarkably small vertical distance between SLG and α-Al_2O_3(0001) at the interface, suggesting the existence of stronger interfacial interactions than van der Waals interactions. *Ab initio* theoretical calculations further demonstrate that the interfacial interactions are electrostatic in nature, which leads to *p*-type doping of SLG, which is consistent with the results of Raman spectroscopy and X-ray photoelectron spectroscopy (XPS). This interaction enables the SLG to slide on the α-Al_2O_3(0001) surface, possibly giving rise to a honeycomb-like network of wrinkles, as observed by atomic force microscopy (AFM).

2 Experimental and calculation method

The graphene was grown on an α-Al_2O_3(0001) substrate in a quartz tube furnace with a base pressure of 2×10^{-6} Pa. The α-Al_2O_3(0001) substrates were annealed at 1,173 K for 60 min in open air to prepare an atomically flat surface. Immediately prior to deposition, the substrates were introduced into the vacuum furnace and then heated to 873 K in vacuum for degassing. Subsequently, the SLG was grown by exposing the sapphire surface to methanol vapor at a pressure of 350 Pa for 120 min at the substrate temperature of 1,273 K. Following growth, the SLG was characterized using a micro-Raman spectrometry. The Raman spectra from the laser spot (which was less than 1 μm in diameter) on the sample were collected with an excitation wavelength of 488 nm in back-scattering geometry. The surface morphology and in-plane atomic structure of the graphene were analyzed via AFM and reflection high-energy electron diffraction (RHEED). XPS and NIXSW spectroscopic analyses were carried out at the BL-27A station of the Photon Factory in the High Energy Accelerator Research Organization (KEK-PF). The measurements were performed with a hemispherical energy analyzer (VSW CLASS-100). The NIXSW profiles were obtained by recording the Al 1*s*, O 1*s*, and C 1*s* photoelectron yields as the incident photon energy was scanned through the Bragg energy. The photon energy scanning causes a yield-modulation of the photoelectrons emitted from the relevant atoms in graphene and α-Al_2O_3(0001), since the phase of the standing wave field relative to the α-Al_2O_3(0001) Bragg planes (i.e., the intensity of the electric field at these atoms) changes with the photon energy. This allows us to determine the atomic arrangement at the SLG/α-Al_2O_3(0001) interface precisely.

The *ab initio* calculations of the SLG/α-Al_2O_3(0001) heterostructure were performed using density functional theory (DFT) [16, 17] with the local density approximation (LDA) for the exchange-correlation functional [18] with periodic boundary conditions using the Vienna *Ab initio* Simulation Package [19–21]. Vanderbilt ultrasoft pseudopotentials (PP) [22] were used along with a plane wave basis set, with an energy cutoff of 396 eV. To calculate the equilibrium atomic structures, the Brillouin zone was sampled according to the Monkhorst–Pack scheme [23], which was used with an 8 × 8 × 1 mesh of *k*-space points (and 8 × 8 × 3 in the test bulk case given below). To avoid spurious interactions between neighboring structures in a tetragonal supercell, a vacuum layer of 10 Å was included in the non-periodic direction. Structural relaxation was performed until the forces acting on each atom become less than 0.05 eV/Å. The α-Al_2O_3(0001) substrate was simulated as a 18-Å thick slab with an oxygen-terminated upper surface taking into account of the NIXSW results (see below). The hexagonal graphene unit cell was multiplied by 2 × 2 (giving a total of 8 carbon atoms) to coincide with the substrate unit cell.

The accuracy of the approach was confirmed by calculation of the corresponding characteristics of bulk sapphire. The structural parameters of the Al_2O_3 system were calculated within error of less than 0.05% (compared with the experimental data taken from Ref. [24]; i.e., a_{calc} = 4.7623 Å and a_{exp} = 4.7602(4) Å, c_{calc} = 12.9906 Å and c_{exp} = 12.9933 Å). This comparison between experimentally measured XPS spectra and the distribution of the partial density of states [25] demonstrates good accuracy of the simulated electronic properties. The calculated band gap of the material was E_{calc} = 6.1 eV compared with a measured value of E_{exp} = 7.5–9.5 eV [26–28]; however, this does not impact the results of our study.

3 Results and discussion

Figures 1(a) and 1(b) show a set of Raman spectra of SLG in the SLG/α-Al_2O_3(0001) heterostructure. The two peaks that appear around 1,600 cm^{-1} and 2,700 cm^{-1} are characteristic of the graphitic structure; i.e., the so-called G and 2D peaks, respectively. The Raman spectra collected at different positions on the sample typically show the single component of the 2D peak as in the figure. This indicates that the whole surface of the α-Al_2O_3(0001) substrate was covered uniformly with the SLG [29]. The spectra also show the disorder-related peaks at around 1,360 cm^{-1} and 2,950 cm^{-1}; i.e., the so-called D peak and D + G peaks. Figure 1(c) shows a plot of the positions of G and 2D peaks (Pos(G) and Pos(2D)) collected from the randomly selected areas on the SLG/α-Al_2O_3(0001) and on the SLG flakes on a SiO_2/Si substrate (SLG/SiO_2) prepared by micromechanical exfoliation for comparison. Pos(G) and Pos(2D) were distributed in the range 1,600–1,612 cm^{-1} and 2,706-2,721 cm^{-1}, respectively, in the SLG/α-Al_2O_3(0001) (red circles), and are in the ranges of 1,582-1,593 and 2,687-2,703 cm^{-1}, respectively, in the SLG/SiO_2 (black squares). The distribution of Pos(2D) and Pos(G) exhibited a linear relationship for SLG/SiO_2, which is attributed to the carrier (i.e., hole) concentration due to the unintentional doping from the substrate [30, 31].

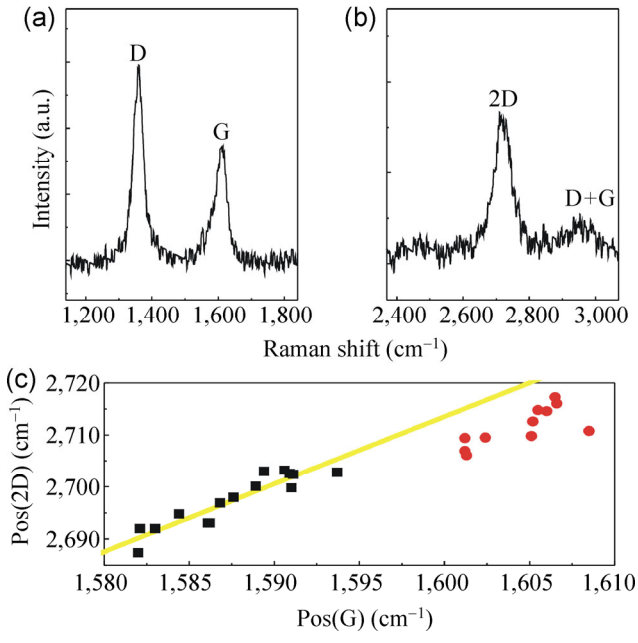

Figure 1 Raman spectra for the (a) D, G and (c) 2D bands of SLG/α-Al_2O_3(001). (c) Plot of Pos(2D)vs. Pos(G). The data-points were measured at randomly selected areas on the SLG/α-Al_2O_3(0001) sample and on SLG/SiO_2 [30] obtained by micromechanical exfoliation. The symbols ■(black) and ●(red) denote the experimental data obtained from Raman spectra of SLG/SiO_2 and SLG/α-Al_2O_3(0001), respectively. The yellow line is plotted assuming linear extrapolation from the data points shown by the black squares.

The larger wavenumbers for Pos(G) and Pos(2D) in the SLG/α-Al_2O_3(0001) exhibited anapproximately linear relationship, which is similar to the SLG/SiO_2 interface, but the deviation from the extrapolated linear fit suggestsa higher hole concentration. There are two factors that may influence the locations of the peaks in addition to doping. The first is the introduction of defects, such as grain boundaries [32–34], and another is chemical interactions with the substrate [35]. It has been reported that the appearance of a new peak (D′ peak) at around 1,620 cm^{-1} results in an upward shift of the G peak in nanocrystalline graphitic structures [33], whereas no obvious upward shift has been reported for the 2D peak in nanocrystalline graphene. The second is that it has been reported that chemical interactions at the interfaces lead to considerable deviation of Pos(2D) and Pos(G) from the linear relationship for SLG/SiO_2 [35]. This second effect, however, can be ruled out based on the NIXSW results (see below). It is clear that a higher hole concentration and greater defect density in SLG are responsible for the higher Pos(G) and Pos(2D) in the SLG/α-Al_2O_3(0001), which follows form considering the appearance of the intense D and D + G peaks.

Figure 2(a) shows RHEED patterns before and after the SLG growth on the α-Al_2O_3(0001) substrate. The directions of the incident electron beam were parallel to the $[10\bar{1}0]$ (i and iii) and $[11\bar{2}0]$ (ii and iv) azimuths of the α-Al_2O_3(0001) substrate, respectively. Following the SLG growth, two sets of streaks appear in the RHEED pattern (see the arrows in Fig. 2(a) (iii) and (iv)). These streaks are attributed to the $[10\bar{1}0]$ and $(11\bar{2}0)$ reflection from SLG, which are equivalent to the corresponding reflections of the three dimensional graphitic structure, because the distance between the neighboring carbon atoms calculated from the spacing of the streak was 1.40 Å, which is consistent with the reported value for graphene obtained by micromechanical exfoliation (1.42 Å) [36]. Figure 2(b) shows an intensity profile along the lines (see Fig. 2(a)) parallel to the shadow edge for the two incident directions of $[10\bar{1}0]$ and $[11\bar{2}0]$ of α-Al_2O_3(0001). By comparing the line profiles taken before and after the SLG growth, the component from the SLG can be clearly distinguished from the component of the

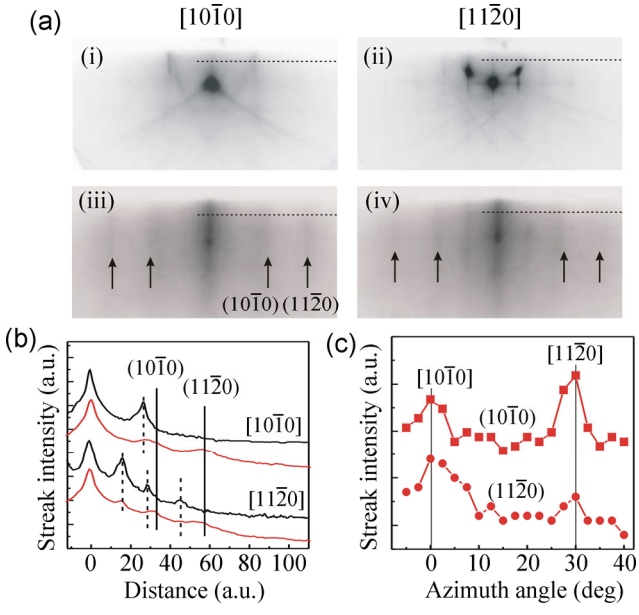

Figure 2 (a) RHEED patterns (i, ii) from α-Al_2O_3(0001) substrate, and (iii, iv) from SLG/α-Al_2O_3(0001). The electrons were incident parallel to the $[10\bar{1}0]$ (left column) and $[11\bar{2}0]$ (right column), respectively. (b) An intensity profile along the dotted lines parallel to the shadow edge for the two incident directions of $[10\bar{1}0]$ and $[11\bar{2}0]$ of α-Al_2O_3(0001). (c) Streak intensities of $[10\bar{1}0]$ and $[11\bar{2}0]$ reflections as a function of the azimuthal angle with respect to the $[10\bar{1}0]$ direction of α-Al_2O_3(0001).

α-Al_2O_3(0001). The streak spacing due to SLG was constant irrespective of the incident direction, as shown by the solid lines for the $(10\bar{1}0)$ and $(11\bar{2}0)$ streaks at the two azimuths. A clear change was observed in the streak intensity depending on the incident direction. In Fig. 2(c), the $(10\bar{1}0)$ and $(11\bar{2}0)$ streak intensities, which were obtained by subtracting a smoothed background from the line profiles, are shown plotted as a function of the azimuth angle with respect to the $[10\bar{1}0]$ direction of α-Al_2O_3(0001). Both the $(10\bar{1}0)$ and $(11\bar{2}0)$ streaks show the maximum intensity at the angles that coincide with the $[11\bar{2}0]$ and $[10\bar{1}0]$ azimuth of α-Al_2O_3(0001). This indicates that SLG is preferably grown with the epitaxial orientations of $[10\bar{1}0]_{SLG}//[11\bar{2}0]_{\alpha\text{-}Al_2O_3(0001)}$, and $[10\bar{1}0]_{SLG}//[10\bar{1}0]_{\alpha\text{-}Al_2O_3(0001)}$.

Figure 3(a) shows an AFM image of SLG/α-Al_2O_3(0001). One can see a honeycomb-like network of wrinkles with mesh sizes of several 100 nm. The height of each wrinkle was less than 0.4 nm, as shown in Fig. 3(b), which is considerably lower than that of graphene/metal heterostructures [37]. It has been

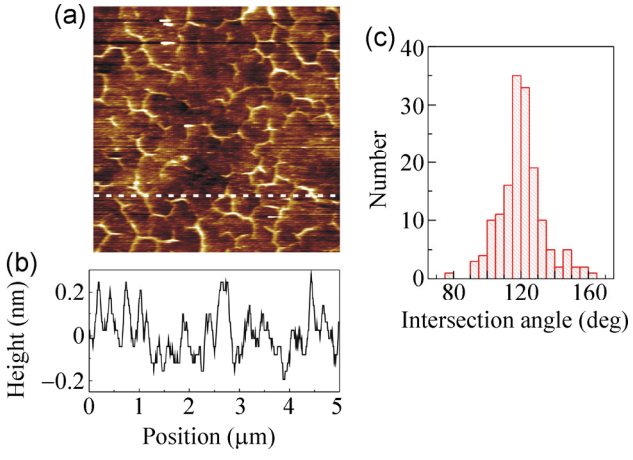

Figure 3 (a) An AFM image of SLG/α-Al_2O_3(0001) and (b) the line profile along the white dotted line in (a). (c) Histogram (the numbers of intersection points) obtained from the AFM analysis, showing the angles of the intersection points of the wrinkles on SLG. The data are from Fig. 3(a).

reported that,with graphene/metal heterostructures, wrinkles are formed due to the difference of the thermal expansion coefficients between graphene and the metal substrate and/or due to the surface roughness of the metal substrate [37]. Note that the angles at the intersections of the wrinkles had a narrow distribution centered at 120°, as shown in Fig. 3(c), which implies long-range stress relaxation in SLG accompanied by wrinkle formation.

Figures 4(a), 4(b), and 4(c) show the standing wave (SW) profiles for the Al, O, and C atomic layers in the SLG/α-Al_2O_3(0001) heterostructure. The Bragg energy was determined as 2,938.5 eV. This energy corresponds to the Bragg diffraction condition from the one sixth of the *c*-axis of α-Al_2O_3 with a lattice spacing of d = 2.17 Å. The SW profile is described by $I(E)/I_0 = 1 + R(E) + 2F[R(E)]^{1/2}\cdot\cos[2\pi d_H - \delta(E)]$, where E is the photon energy, $R(E)$ is the reflectivity of the substrate, $\delta(E)$ is the energy-dependent phase modulation caused by the X-ray standing wave, F is the structure factor, and d_H is the coherent position of the atoms measured from the X-ray scattering plane [14]. The red solid lines in the figures are the best fits to this equation for the respective profiles. These fits give $d_H = -0.1$, $d_H = 0.5$ and $d_H = 1.7$ for Al, O and C, respectively. Thus, the vertical distances of the Al, O and C atoms above the scattering plane, which are obtained by multiplying

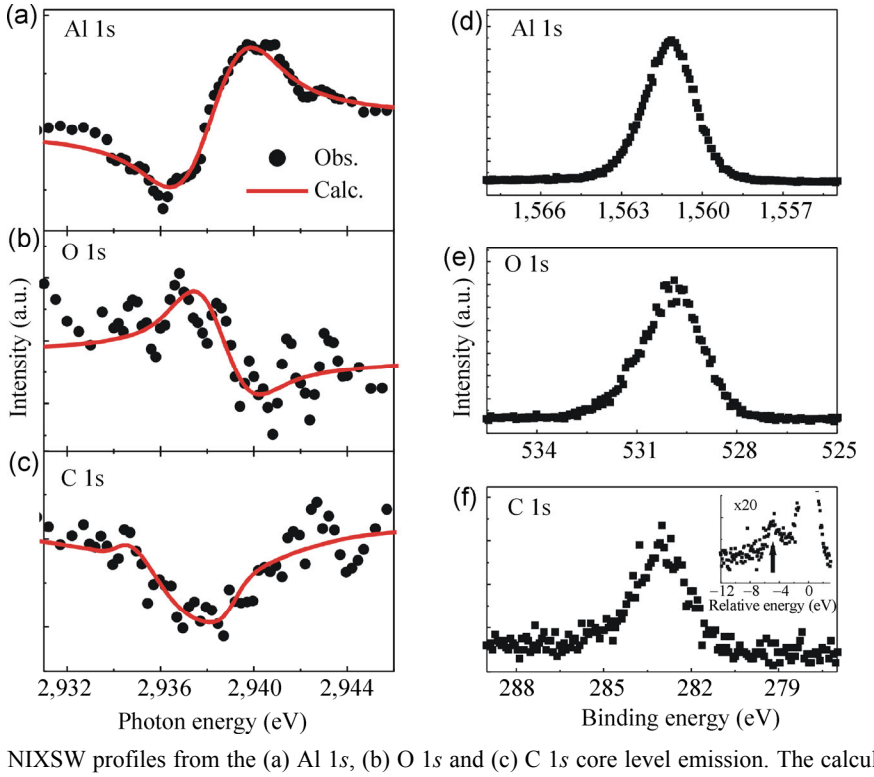

Figure 4 (left panels) NIXSW profiles from the (a) Al 1*s*, (b) O 1*s* and (c) C 1*s* core level emission. The calculated intensity profiles (solid lines) are also included in the figure. (right panels) XPS spectra for the (d) Al 1*s*, (e) O 1*s* and (f) C 1*s* core level regions taken using 3,000 eV photons. The inset in (f) shows the C 1s shake-up spectrum corresponding to the higher binding energy side of the main C 1*s* peak, where the horizontal axis represents the relative energy with respect to the main peak position.

d_H by d, were calculated to be –0.2, 1.1, and 3.7 Å, respectively.

Table 1 lists a summary of these data with the DFT calculation results (see below). Two possible arrangements of the Al and O atomic layers in the interfacial region can be considered in accordance with these values, which are the structures corresponding to the oxygen or aluminum termination on the surface of α-Al_2O_3(0001). We estimate that the former and latter arrangements have the vertical distances of 2.6 Å and 3.9 Å between SLG and the topmost O and Al layer of α-Al_2O_3(0001), respectively. The latter possibility, however, can be eliminated since the distance is much larger than the interlayer distance of graphite (3.356 Å) [38] and the vertical distance between SLG–Ir(111) (3.38 Å) [39] is expected for weak interfacial interactions due to van der Waals forces. The SLG–α-Al_2O_3(0001) distance (2.6 Å) is larger than the SLG–Ni(111) distance (2.15 Å) [40] with covalent interactions; however, is much smaller than the separations with van der Waals interactions.

Figures 4(d), 4(e), and 4(f) show the Al 1*s*, O 1*s*, and C 1*s* XPS spectra of the SLG/α-Al_2O_3(0001) heterostructure, respectively. The C 1*s* shake-up spectrum is also shown in the inset of Fig. 4(f). The binding energies of the Al 1*s* and O 1*s* core levels associated with the α-Al_2O_3(0001) substrate were almost identical to the previously reported values for sapphire [41]. In contrast, the C 1*s* binding energy of SLG (283.1 eV) was shifted to the lower energies by –1.3 eV compared with that of graphite (284.4 eV [42]). The C 1*s* binding energy of SLG has been reported to show a considerable dependence on the substrate; i.e., 285.1 eV for SLG/Ni(111) [43], 284.0 eV for SLG/Pt(111) [44] and 284.2 eV for SLG/Ir(111) [45]; however, the energy shifts from that in graphite are much smaller than 1 eV. In the C 1*s* shake-up spectrum, a single peak is seen at around –5 eV (indicated by arrow in the inset of Fig. 4(f)). This peak is attributed to the π-plasmon excitation of the graphitic structure [46] and carbide formation can be ruled out. Therefore, we may conclude that the unusually large negative C 1*s* binding energy shift observed in this study is due to nonchemical interactions between SLG and sapphire. From the above discussion on the Pos(2D) vsPos(G) relationship in the Raman spectra (see Fig. 1(c)) and on the C 1*s* binding energy shift in XPS, it is clear that SLG on the sapphire surface is *p*-doped and chemical interactions are not dominant at the SLG/α-Al_2O_3(0001) interface.

The DFT calculations provide additional insight into the atomic and electronic structure of the SLG/α-Al_2O_3(0001) interface and the nature of the strong interfacial interactions. In the calculations, the top and bottom surfaces of the sapphire slab were assumed to be terminated by O atoms, considering the atomic arrangements elucidated by NIXSW spectra. Taking account of the RHEED measurements shown in Fig. 2, two atomic arrangements of SLG on α-Al_2O_3(0001) were adopted for the calculations: $[10\bar{1}0]_{SLG}//[11\bar{2}0]_{\alpha\text{-}Al_2O_3(0001)}$ and $[10\bar{1}0]_{SLG}//[10\bar{1}0]_{\alpha\text{-}Al_2O_3(0001)}$. The distance between the neighboring carbon atoms was altered to match the lattice of α-Al_2O_3(0001) substrate. In the first atomic rearrangement, the C–C distance was 1.38 Å, whereas in the second it was 1.51 Å. This approach is justified by a report [47] of a model with strained graphene lattice, which reproduced qualitatively the

Table 1 Vertical distances of the atomic layers of the constituent elements above the X-ray scattering plane (for the NIXSW results) and above the first Al layer (for the DFT results) in the SLG/α-Al_2O_3(0001) interfacial region, and the vertical distances between the SLG film and the α-Al_2O_3(0001) surface estimated from the NIXSW spectroscopy and DFT calculations, respectively

	NIXSW	DFT	
	Interfacial region; vertical distance from scattering plane (Å)	Interfacial region; vertical distance from first Al layer (Å)	
		$[10\bar{1}0]_{SLG}//[11\bar{2}0]_{\alpha\text{-}Al_2O_3(0001)}$	$[10\bar{1}0]_{SLG}//[10\bar{1}0]_{\alpha\text{-}Al_2O_3(0001)}$
Al	–0.2	0	0
O	1.1	1.2	1.1
C	3.7	4.1	3.8
SLG/α-Al_2O_3(0001)	2.6	2.9	2.7

main features of the surface electronic structure.

Figures 5 (a) and 5(b) show the calculated atomic structure of SLG/α-Al_2O_3(0001). The calculations give the vertical distance of 2.9 Å for $[10\bar{1}0]_{SLG}//[11\bar{2}0]_{\alpha\text{-}Al_2O_3(0001)}$ (Fig. 5(a)) and 2.7 Å for $[10\bar{1}0]_{SLG}//[10\bar{1}0]_{\alpha\text{-}Al_2O_3(0001)}$ (Fig. 5(b)) between SLG and the topmost O layer of α-Al_2O_3(0001), which is consistent with the experimentally measured value of 2.6 Å.

The vertical distance between SLG and the first Al layer were found to be 4.1 Å and 3.8 Å and that between the topmost O layer and the first Al layer was found to be 1.2 Å and 1.1 Å for the two atomic arrangements, respectively. These are consistent with the experimentally measured values of 3.9 Å and 1.3 Å, respectively (see Table 1). Note that the interactions with SLG lead to a slight decrease in the vertical distance between the topmost O layer and the first Al layer from 1.23 Å to 1.1–1.2 Å, which suggests that relaxation of the interfacial structure has occurred.

Calculations of the charge density in the SLG/α-Al_2O_3(0001) system are shown in Figs. 5(c) and 5(e), which allow us to gain insight into the nature of the interfacial interactions. Figures 5(d) and 5(f) show the difference in the charge density between the SLG/α-Al_2O_3(0001) heterostructure and the freestanding sapphire and freestanding SLG; these data show that the interactions between the SLG and sapphire are physical in nature, and originate from the electrostatic interactions between graphene and the topmost O atoms of α-Al_2O_3(0001). The electrostatic interactions between SLG and α-Al_2O_3(0001) for both arrangements can be understood form Fig. 6(a), which shows the partial densities of states of SLG and sapphire in SLG/α-Al_2O_3(0001) compared with those of the freestanding SLG and sapphire slabs. In SLG/α-Al_2O_3(0001), the Dirac point of graphene is shifted to 1.1–1.3 eV

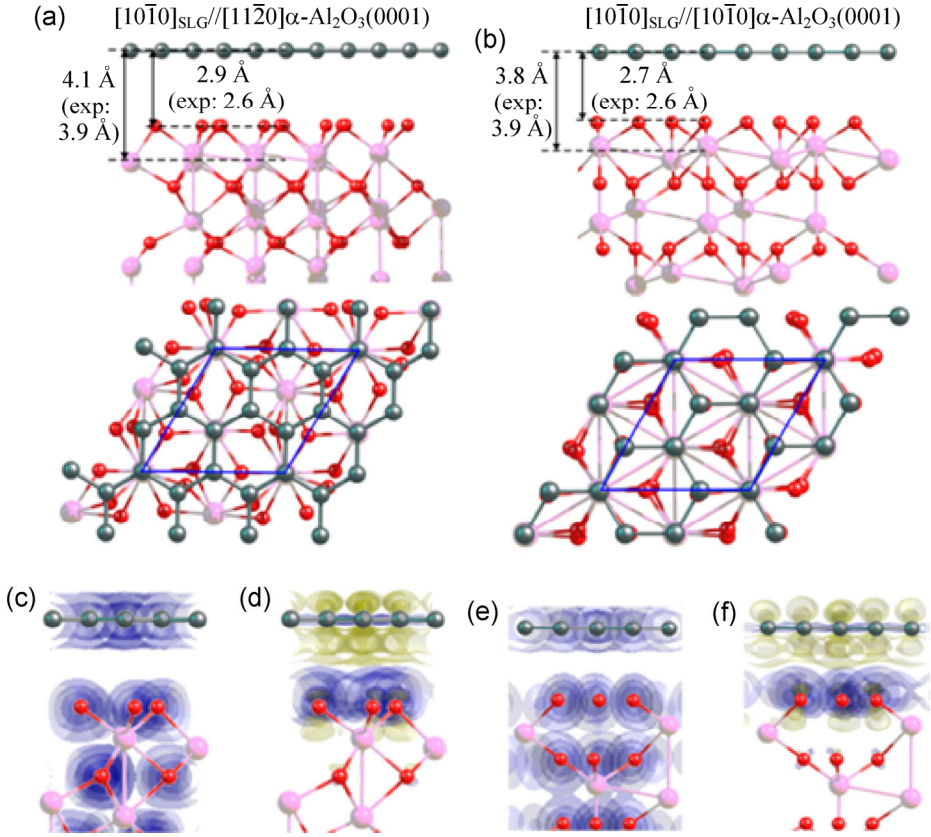

Figure 5 (a,b) Atomic structure, (c,e) spatial charge density distribution, and (d,f) the difference in the spatial charge density distribution between the SLG/α-Al_2O_3(0001) system and the free-standing SLG and sapphire slabs for SLG/α-Al_2O_3(0001) for $[10\bar{1}0]_{SLG}//[11\bar{2}0]_{\alpha\text{-}Al_2O_3(0001)}$, and $[10\bar{1}0]_{SLG}//[10\bar{1}0]_{\alpha\text{-}Al_2O_3(0001)}$ arrangements. C, O, and Al atoms are marked by dark green, red, and pink, respectively. In (a) and (b) the experimental data are shown in parentheses. In (d) and (f), the loss and the gain of the charge are shown by the yellowish and bluish colors, respectively.

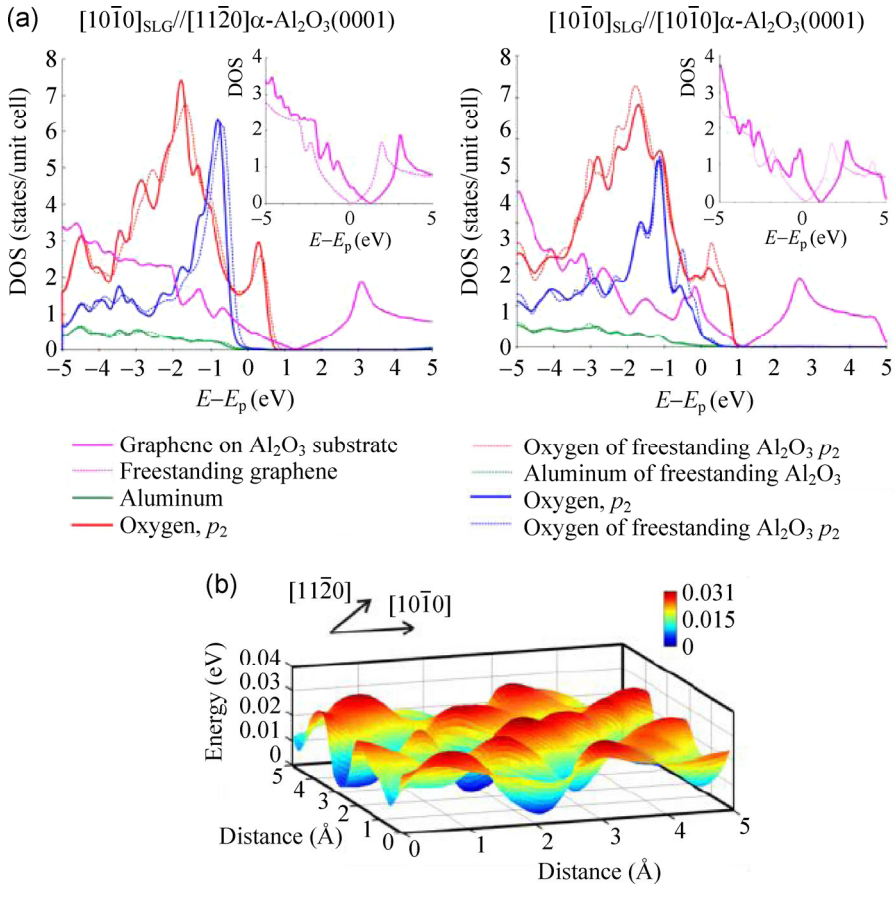

Figure 6 (a) Partial density of states of p_z orbitals of graphene (pink), the first Al layer (green) and the topmost O layer, which is decomposed into p_{xy} and p_z orbitals (red and purple, respectively), for SLG/α-Al_2O_3(0001) (solid lines) and freestanding α-Al_2O_3(0001) (dotted lines). The two insets show the partial density of states of p_z orbitals of graphene in SLG/α-Al_2O_3(0001) (pink solid line) and in the free-standing SLG (pink dotted line). The calculated results shown in the left and right panels reflect the atomic arrangements of $[10\bar{1}0]_{SLG}//[11\bar{2}0]_{\alpha\text{-}Al_2O_3(0001)}$ and $[10\bar{1}0]_{SLG}//[10\bar{1}0]_{\alpha\text{-}Al_2O_3(0001)}$, respectively. (b) Potential energy surface for SLG migration on α-Al_2O_3(0001). The arrows represent $[10\bar{1}0]$ and $[11\bar{2}0]$ directions. The two-dimensional changes in the energy are shown via color-index.

relative to the freestanding case (see the insets of Fig. 6(a)). This result is consistent with p-type doping of the graphene structure due to the interaction with the substrate. The magnitude of the shift is comparable with that reported for graphene on oxygen-terminated SiO_2 (i.e., 1 eV) [12].

The distortion of carbon p_z orbitals in the region of –1 eV, where the surface oxygen p_z orbitals are located, indicates the presence of strong electrostatic interactions between SLG and α-Al_2O_3(0001), which are attributed mainly to coupling between the graphene π system and the unsaturated p_z electrons of the topmost O layer. The adhesion energy of SLG on α-Al_2O_3(0001) was estimated to be 0.11 and 0.13 eV/carbon for $[10\bar{1}0]_{SLG}//[10\bar{1}0]_{\alpha\text{-}Al_2O_3(0001)}$ and $[10\bar{1}0]_{SLG}//[11\bar{2}0]_{\alpha\text{-}Al_2O_3(0001)}$, respectively. These energies are comparable to those reported for SLG on metals, i.e., 0.16–0.18 eV/carbon for Co [48, 49], 0.12–0.13 eV/carbon for Ni [48–51], and 0.14 eV/carbon for Ru [51].

The calculations of the adhesion energy depend on the lateral position of the SLG on α-Al_2O_3(0001), and allow the construction of a potential energy surface, as shown in Fig. 6(b). This provides information about SLG migration on α-Al_2O_3(0001), including an energy barrier for migration. The electrostatic nature of the interfacial interactions associated with the relatively uniform π system of graphene without the influence of chemical bonding leads to a small migration barrier of around 0.03 eV from the energetically favorable state (see Fig. 5(a)), as shown in Fig. 6(b).

The small migration barrier for SLG/α-Al_2O_3(0001) allows the SLG to "slide" on the surface, despite the strong interfacial interactions, as indicated by the small vertical distance between SLG and α-Al_2O_3(0001). It has been demonstrated that the atomic arrangement of SLG on α-Al_2O_3(0001) is strongly dependent on the growth temperature [4, 5, 8]. Fanton *et al.* pointed out that 1,550 °C is required for van der Waals epitaxy [5]. Hwang *et al.* have demonstrated that a single dominant SLG crystal can be obtained via a two-step growth process, which consists of a low-temperature nucleation at 1,250–1,350 °C followed by growth at higher temperature of 1,450–1,650 °C [8]. In this work, although single-crystalline epitaxial growth was not realized in SLG/α-Al_2O_3(0001), two preferred orientations were clearly observed even at the lower growth temperature of 1,000 °C. This is attributed to the growth mechanism of SLG on α-Al_2O_3(0001), which is affected by the interfacial interactions. This might also enable relaxation of the thermal stressesover a large area, which results in the honeycomb-like network of wrinkles, possibly during the cooling of the sample following CVD growth. For comparison, the migration barrier of SLG has been reported to be as large as 0.08 eV for SLG/Ni(111), where the SLG exhibits epitaxial growth on the Ni(111) surface [11] and gives rise to much larger and more irregularly distributed wrinkles [37], which is in contrast to the SLG/α-Al_2O_3(0001) system.

4 Conclusion

The atomic structure and electronic properties of SLG directly grown on α-Al_2O_3(0001) have been investigated experimentally and theoretically. The analysis of the in-plane atomic arrangement of SLG on α-Al_2O_3(0001) shows that SLG grows with two distinct preferred orientations, i.e., $[10\bar{1}0]_{SLG}//[11\bar{2}0]_{\alpha\text{-}Al_2O_3(0001)}$ and $[10\bar{1}0]_{SLG}//[10\bar{1}0]_{\alpha\text{-}Al_2O_3(0001)}$ in the polycrystalline grains. The graphene atomic planes face the oxygen atoms, which constitute the topmost layer of α-Al_2O_3(0001) at the interface. The vertical distance between the graphene layer and the α-Al_2O_3(0001) was found to be 2.6 Å, which is considerably smaller than that expected for van der Waals interactions, and indicates that the system exhibits strong interfacial interactions.

The electronic properties, measured via micro-Raman spectroscopy and XPS, also support the above strong interactions due to the evidence for *p*-type doping in SLG. The DFT calculations were able to reproduce the experimental results accurately, and provide evidence for the electrostatic interactions between the graphene π system and the unsaturated p_z electrons of the topmost O layer, whichleads strong interfacial interactions at the SLG/α-Al_2O_3(0001) interface. The small migration barrier originating from the electrostatic interactions may give rise to the appearance of two atomic arrangements, and a honeycomb-like network of wrinkles in the SLG film at the macroscopic scale through easy sliding of SLG.

This work provides an important basis for a comprehensive understanding of the growth mechanism of graphene on sapphire substrates, as well as precise control of the electrical properties of graphene, which is required to manufacture high performance electronic and spintronic devices.

Acknowledgements

We are grateful to the 'Chebishev' and 'Lomonosov' supercomputers of Moscow State University for providing the chance of using a cluster computer for quantum-chemical calculations. S.E. thanks Prof. H. Kondo (Keio University) and Prof. T. Shimada (Hirosaki University) for NIXSW measurements. This work was partly supported by Grants-in-Aid for Young Scientists B (Grant No. 22760033) from the Japan Society for the Promotion of Science. The present work has been performed under the approval of the Photon Factory Program Advisory Committee (PF PAC Nos. 2010G660 and 2012G741). P.V.A., P.B.S. and L.Y.A. acknowledge the support from the Russian Science Foundation (project No. 14-13-00139).

References

[1] Novoselov, K. S.; Geim, A. K.; Morozov, S. V.; Jiang, D.; Zhang, Y.; Dubonos, S. V.; Grigorieva, I. V.; Firsov, A. A. Electric field effect in atomically thin carbon films. *Science* **2004**, 306, 666–669.

[2] Zhang, Y. B.; Tan, Y. W.; Stormer, H. L.; Kim, P. Experimental observation of the quantum Hall effect and Berry's phase in graphene. *Nature* **2005**, 438, 201–204.

[3] Heersche, H. B.; Jarillo-Herrero, P.; Oostinga, J. B.; Vandersypen, L. M. K.; Morpurgo, A. F. Bipolar supercurrent in graphene. *Nature* **2007**, 446, 56–59.

[4] Hwang, J.; Shields, V. B.; Thomas, C. I.; Shivaraman, S.; Hao, D.; Kim, M.; Woll, A. R.; Tompa, G. S.; Spencer, M. G. Epitaxial growth of graphitic carbon on C-face SiC and sapphire by chemical vapor deposition (CVD). *J. Cryst. Growth* **2010**, 312, 3219–3224.

[5] Fanton, M. A.; Robinson, J. A.; Puls, C.; Liu, Y.; Hollander, M. J.; Weiland, B. E.; LaBella, M.; Trumbull, K.; Kasarda, R.; Howsare, C. et al. Characterization of graphene films and transistors growth on sapphire by metal-free chemical vapor deposition. *ACS Nano* **2011**, 5, 8062–8069.

[6] Song, H. J.; Son, M.; Park, C.; Lim, H.; Levendorf, M. P.; Tsen, A. W.; Park, J.; Choi, H. C. Large scale metal-free synthesis of graphene on sapphire and transfer-free device fabrication. *Nanoscale* **2012**, 4, 3050–3054.

[7] Nakamura, A.; Miyasaka, Y.; Temmyo, J. Direct growth properties of graphene layers on sapphire substrate by alcohol-chemical vapor deposition. *Jpn. J. Appl. Phys.* **2012**, 51, 04DN03.

[8] Hwang, J.; Kim, M.; Campbell, D.; Alsalman, H. A.; Kwak, J. Y.; Shivaraman, S.; Woll, A. R.; Singh, A. K.; Hennig, R. G.; Gorantla, S.et al. Van der waals epitaxial growth of graphene on sapphire by chemical vapor deposition without a metal catalyst. *ACS Nano* **2013**, 7, 385–395.

[9] Novoselov, K. S.; Jiang, D.; Schedin, F.; Booth, T. J.; Kohtkevich, V. V.; Morozov, S. V.; Geim, A. K. Two-dimensional atomic crystals. *PNAS* **2005**, 102, 10451–10453.

[10] Li, X. S.; Cai, W. W.; An, J. H.; Kim, S.; Nah, J.; Yang, D. X.; Piner, R.; Velamakanni, A.; Jung, I.; Tutuc, E.; et al. Large-area synthesis of high-quality and uniform graphene films on copper foils. *Science* **2009**, 324, 1312–1314.

[11] Entani, S.; Matsumoto, Y.; Ohtomo, M.; Avramov, P. V.; Naramoto, H.; Sakai, S. Precise control of single- and bi-layer graphene growths on epitaxial Ni(111) thin film. *J. Appl. Phys.* **2012**, 111, 064324.

[12] Chen, K.; Wang, X. M.; Xu, J. B. Electronic properties of graphene altered by substrate surface chemistry and externally applied electric field. *J. Phys. Chem. C***2012**, 116, 6259–6267.

[13] Du, A. J.; Ng, H. H.; Bell, N. J.; Zhu, Z. H.; Amal, R.; Smith, S. C. Hybrid graphene/titaniananocomposite: interface charge transfer, hole doping, and sensitization for visible light response. *J. Phys. Chem. Lett.* **2011**, 2, 894–899.

[14] Woodruff, D. P.; Seymour, D. L.; McConvill, C. F.; Riley, C. E.; Crapper, M. D.; Prince, N. P.; Jones, R. G. Simple X-ray standing-wave technique and its application to the investigation of the Cu(111) ($\sqrt{3}\times\sqrt{3}$)*R*30°-Cl structure. *Phys. Rev. Lett.* **1987**, 58, 1460–1462.

[15] Baba, Y.; Narita, A.; Sekiguchi, T.; Shimoyama, I.; Hirao, N.; Entani, S.; Sakai, S. Structure determination of self-assembled monolayer on oxide surface by soft-X-ray standing wave. *e-J. Surf. Sci. Nanotech.* **2012**, 10, 69-73.

[16] Hohenberg, P.; Koh, W. Inhomogeneous electron gas. *Phys. Rev.* **1964**, 136, B864–B871.

[17] Kohn, W.; Sham, L. J. Self-consistent equations including exchange and correlation effects. *Phys. Rev.* **1965**, 140, A1133–A1138.

[18] Ceperley, D. M.; Alder, B. J. Ground state of the electron gas by a stochastic method. *Phys. Rev. Lett.* **1980**, 45, 566–569.

[19] Kresse, G.; Hafner, J. *Ab initio* molecular dynamics for liquid metals. *Phys. Rev. B***1993**, 47, 558–561.

[20] Kresse, G.; Hafner, J. *Ab initio* molecular-dynamics simulation of the liquid-metal-amorphous-semiconductor transition in germanium. *Phys. Rev. B***1994**, 49, 14251–14269.

[21] Kresse, G.; Furthmüller, J. Efficient iterative schemes for *ab initio* total-energy calculations using a plane-wave basis set. *Phys. Rev. B***1996**, 54, 11169–11186.

[22] Vanderbilt, D. Soft self-consistent pseudopotentials in a generalized eigenvalue formalism. *Phys. Rev. B***1990**, 41, 7892–7895.

[23] Monkhorst, H. J.; Pack, J. D. Special points for Brillouin-zone integrations. *Phys. Rev. B***1976**, 13, 5188–5192.

[24] Lewis, J.; Schwarzenbach, D.; Flack, H. D. Electric field gradients and charge density in corundum, α-Al_2O_3. *Acta Cryst.* **1982**, A38, 733–739.

[25] Perevalov, T. V.; Shaposhnikov, A. V.; Gritsenko, V. A.; Wong, H.; Han, J. H.; Kim, C. W. Electronic structure of α-Al_2O_3: ab initio simulations and comparison with experiment. *JETP Lett.* **2007**, 85, 165–168.

[26] Arakawa, E. T.; Williams, M. W. Optical properties of aluminum oxide in the vacuum ultraviolet. *J. Phys. Chem. Solids.* **1968**, 29, 735–744.

[27] Balzarotti, A.; Bianconi, A. Electronic structure of aluminium oxide as determined by X-ray photoemission. *Phys. Status. Solidi B* **1976**, 76, 689–694.

[28] French, R. H. Electronic band structure of Al_2O_3, with comparison to AlON and AlN. *J. Am. Ceram. Soc.* **1990**, 73, 477–489.

[29] Ferrari, A. C.; Meyer, J. C.; Scardaci, V.; Casiraghi, C.; Lazzeri, K.;, Marui, F.; Piscanec, S.; Jiang, D.; Novoselov, K. S.; Roth, S. et al. Raman spectrum of graphene and graphene layers. *Phys. Rev. Lett.* **2006**, 97, 187401.

[30] Yan, J.; Zhang, Y. B.; Kim, P.; Pinczuk, A. Electric field effect tuning of electron-phonon coupling in graphene.*Phys. Rev. Lett.* **2007**, 98, 166802.

[31] Pisana, S.; Lazzeri, M.; Casiraghi, C.; Novoselov, K. S.; Geim, A. K.; Ferrari, A. C.; Mauri, F. Breakdown of the adiabatic Born-Oppenheimer approximation in graphene. *Nat. Mater.* **2007**, 6, 198–201.

[32] Lespade, P.; Marchand, A.; Couzi, M; Cruege, F. Caracterisation de materiaux carbones par microspectro-metrieraman. *Carbon* **1984**, 22, 375–385.

[33] Ferrari, A. C.; Robertson, J. Interpretation of raman spectra of disordered and amorphous carbon. *Phys. Rev. B***2000**, 61, 14095.

[34] Casiraghi, C.; Pisana, S.; Novoselov, K. S.; Geim, A. K.; Ferrari, A. C. Raman fingerprint of charged impurities in graphene. *Appl. Phys. Lett.* **2007**, 91, 233108.

[35] Entani, S.; Sakai, S.; Matsumoto, Y.; Naramoto, H.; Hao, T.; Maeda, Y. Interface properties of metal/graphene heterostructures studied by micro-raman spectroscopy. *J. Phys. Chem. C***2010**, 114, 20042–20048.

[36] Gass, M. H.; Bangert, U.; Bleloch, A. L.; Wang, P.; Nair, R. R.; Geim, A. K. Free-standing graphene at atomic resolution. *Nat. Nanotechnol.* **2008**, 3, 676–681.

[37] Chae, S. J.; Günes, F.; Kim, K. K.; Kim, E. S.; Han, G. H.; Kim, S. M.; Shin, H.; Yoon, S.; Choi, Y.; Park, M. H. et al. Synthesis of large-area graphene layers on poly-nickel substrate by chemical vapor deposition: Wrinkle formation. *Adv. Mater.* **2009**, 21, 2328–2333.

[38] Trucano, P.; Chen, R. Structure of graphite by neutron diffraction. *Nature* **1975**, 258, 136–137.

[39] Busse, C.; Lazić, P.; Djemour, R.; Coraux, J.; Gerber, T.; Atodirescei, N.; Caciuc, V.; Brako, R.; N'Diaye, A. T.; Blügel, S. et al. Graphene on Ir(111): Physisorption with chemical modulation. *Phys. Rev. Lett.* **2011**, 107, 036101.

[40] Gamo, Y.; Nagashima, A.; Wakabayashi, M.; Terai, M.; Oshima, C. Atomic structure of monolayer graphite formed on Ni(111). *Surf. Sci.* **1997**, 374, 61–64.

[41] Wagner, C. D. X-ray photoelectron spectroscopy with x-ray photons of higher energy. *J. Vac. Sci. Technol.* **1978**, 15, 518–523.

[42] Hamrin, K.; Johansson, G.; Gelius, U.; Nordling, C.; Siegbahn, K. Valence bands and core levels of the isoelectronic series LiF, BeO, BN, and graphite studied by ESCA. *Phys. Scripta.* **1970**, 1, 277–280.

[43] Nagashima, A.; Tejima, N.; Oshima, C. Electronic states of the pristine and alkali-metal-intercalated monolayer graphite/Ni(111) systems. *Phys. Rev. B***1994**, 50, 17487–17495.

[44] Entani, S.; Ikeda, S.; Kiguchi, M.; Saiki, K.; Yoshikawa, G.; Nakai, I.; Kondoh, H.; Ohta, T. Growth of nanographite on Pt(111) and its edge state. *Appl. Phys. Lett.* **2006**, 88, 153126.

[45] Preobrajenski, A. B.; Ng, N. L.; Vinogradov, A. S.; Mårtensson, N. Controlling graphene corrugation on lattice-mismatched substrates.*Phys. Rev. B***2008**, 78, 073401.

[46] Eberlein, T.; Bangert, U. B.; Nair, R. R.; Jones, R.; Gass, M.; Bleloch, A. L.; Novoselov, K. S.; Geim, A.; Briddon, P. R. Plasmon spectroscopy of free-standing graphene films. *Phys. Rev. B***2008**, 77, 233406.

[47] Stradi, D.; Barja, S.; Díaz, C.; Barnica, M.; Borca, B.; Hinarejos, J. J.; Sánchez-Portal, D.; Alcamí, M.; Arnau, A.; Vázquez de Parga, A. L.; Miranda, R.; Martín, F. Lattice-matched versus lattice-mismatched models to describe epitaxial monolayer graphene on Ru(0001). *Phys. Rev. B***2013**, 88, 245401.

[48] Giovannetti, G.; Khomyakov, P. A.; Brocks, G.; Karpan, V. M.; van den Brink, J.; Kelly, P. J. Doping graphene with metal contacts. *Phys. Rev. Lett.* **2008**, 101, 026803.

[49] Vanin, M.; Mortensen, J. J.; Kelkkanen, A. K.; Garcia-Lastra, J. M.; Thygesen, K. S.; Jacobsen, K. W. Graphene on metals: A van der Waals density functional study. *Phys. Rev. B***2010**, 81, 081408.

[50] Kozlov, S. M.; Viñes, F.; Görling, A. Bonding mechanisms of graphene on metal surfaces. *J. Phys. Chem. C***2012**, 116, 736.

[51] Gong, C.; Lee, G.; Shan, B.; Vogel, E. M.; Wallace, R. M.; Cho, K. First-principles study of metal-graphene interface. *J. Appl. Phys.* **2010**, 108, 123711.